Thermoreversible Control of Nucleic Acid Structure and Function with Glyoxal Caging

Steve D. Knutson‡, Aimee A. Sanford‡, Colin S. Swenson, Megan M. Korn, Brea A. Manuel and Jennifer M. Heemstra

Department of Chemistry, Emory University, Atlanta, Georgia 30322, United States

ABSTRACT: Controlling the structure and activity of nucleic acids dramatically expands their potential for application in therapeutics, biosensing, nanotechnology and biocomputing. Several methods have been developed to impart responsiveness of DNA and RNA to small-molecule and light-based stimuli. However, heat-triggered control of nucleic acids has remained largely unexplored, leaving a significant gap in responsive nucleic acid technology. Moreover, current technologies have been limited to natural nucleic acids and are often incompatible with polymerase-generated sequences. Here we show that glyoxal, a well-characterized compound that covalently attaches to the Watson-Crick-Franklin face of several nucleobases, addresses these limitations by thermoreversibly modulating the structure and activity of virtually any nucleic acid scaffold. Using a variety of DNA and RNA constructs, we demonstrate that glyoxal modification is easily installed and potently disrupts nucleic acid structure and function. We also characterize the kinetics of decaging and show that activity can be restored via tunable thermal removal of glyoxal adducts under a variety of conditions. We further illustrate the versatility of this approach by reversibly caging a 2'-*O*-methylated RNA aptamer as well as synthetic threose nucleic acid (TNA) and peptide nucleic acid (PNA) scaffolds. Glyoxal caging can also be used to reversibly disrupt enzyme-nucleic acid interactions, and we show that caging of guide RNA allows for tunable and reversible control over CRISPR-Cas9 activity. We also demonstrate glyoxal caging as an effective method for enhancing PCR specificity, and we cage a biostable antisense oligonucleotide for time-release activation and titration of gene expression in living cells. Together, glyoxalation is a straightforward and scarless method for imparting reversible thermal responsiveness to theoretically any nucleic acid architecture, addressing a significant need in synthetic biology and offering a versatile new tool for constructing programmable nucleic acid components in medicine, nanotechnology and biocomputing.

Introduction

Nucleic acids are highly versatile and dynamic biomolecules, exhibiting large data storage capacity and a high degree of structural complexity, in turn endowing them with diverse molecular recognition and catalytic activities. These attractive properties explain their ubiquitous presence in Nature and warrant investigation of nucleic acids as programmable synthetic components in biomedicine, nanotechnology and biocomputing.[1-4] Just as Nature engages temporal and spatial regulation to control gene expression, achieving tunable and predictable control over the structure and activity of nucleic acid constructs *in vitro* is vital toward their use in synthetic biology and biotechnology applications.

Several approaches have been explored to impart stimuli-responsive properties to nucleic acids and facilitate external control over their structure and function. Early methods to achieve chemically-triggered activation of nucleic acids incorporated trichloroethyl[5] or 4-nitrobenzyl[6] groups during solid-phase oligonucleotide synthesis. Resulting adducts prevent duplex formation and higher-order assembly, and can be subsequently removed by reducing agents, including zinc/acetic acid mixtures or sodium thiosulfate. Photoreversible blocking strategies have also been developed.[7-14] Similar to these previous methods, "photocaged" nucleobase derivatives are incorporated into oligonucleotide synthesis workflows, and can be uncaged with UV light to restore nucleic acid function. While effective, these protecting groups must be incorporated during oligonucleotide synthesis and are thus only applicable to relatively short strands. Moreover, the difficulty and cost of synthesizing these modified phosphoramidite monomers can be limiting, and thus it is essential to have information about the key residues to be caged in order to mask the activity of the sequence. More recent "cloaking" methods employ acylation of 2' hydroxyls in RNA with either an azide-containing or *o*-nitroveratryl photoreactive reagent, which are then respectively removed by triphosphine-mediated Staudinger reduction or light-triggered decaging.[15-16] While these methods allow caging of both chemically and enzymatically synthesized transcripts, these acylation reagents can only be applied to RNA, and no comparable methods are available for other nucleic acid scaffolds. Additionally, achieving full reactivation of cloaked RNA constructs can be challenging,[15-16] and UV removal of adducts in particular can both impart structural changes to certain nucleobases[17] and further require specialized and costly instrumentation.

In contrast to chemical or light-driven approaches, we envisioned that temperature could offer a straightforward external stimulus for controlling the caging of nucleic acids. Heat is relatively easy to introduce in a variety of settings, and a number of laboratory instruments that precisely control temperature are both commonplace and economical. Despite these advantages, heat-sensitive caging of nucleic acids remains

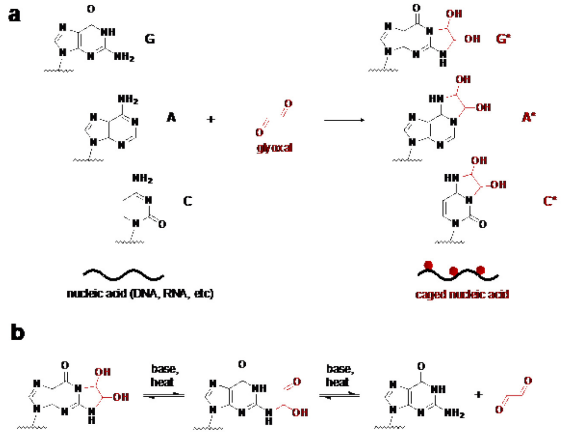

Figure 1. Glyoxal reactivity with nucleobases. a) Glyoxal forms *bis*-hemiaminal adducts (*) on guanine (G), adenosine (A), and cytidine (C) nucleobases. b) Glyoxal decaging occurs upon addition of heat under mild alkaline conditions.

largely unexplored. To address this need, we recognized that glyoxal could serve as an effective thermoresponsive caging group. Glyoxal reacts readily with nitrogen groups on the Watson-Crick-Franklin face of nucleobases to produce stable *bis*-hemiaminal adducts, and this reaction has been demonstrated in both RNA and DNA. Guanosine addition is typically the most stable and rapidly formed product, but longer reaction times (>30 min) and higher glyoxal concentrations (>0.1 M) can also lead to reaction of adenosine and cytidine (Figure 1a).[18-22] Adduct formation directly interferes with base pairing, and thus denatures overall secondary structure in nucleic acids. Attesting to the convenience and efficacy of this reaction, glyoxal has been utilized for several decades in electrophoresis analysis and structural probing of large RNAs,[23-24] and glyoxal can be used as a potent cell and tissue fixative prior to immunohistochemical staining.[25] Kethoxal, a chemical derivative of glyoxal, has also found broad utility for high-throughput mapping of RNA secondary structure.[26]

Key to use of glyoxal as a nucleic acid caging reagent is the ability to reverse adduct formation and restore base pairing. Fortuitously, glyoxal can be easily deprotected through a combination of heat and mild alkaline conditions (Figure 1b).[27] Taken together, the previous applications of glyoxal highlight several unique properties that we recognized could be leveraged for thermoresponsive caging: (1) glyoxalation is sufficient to disrupt strong nucleic acid secondary structure, (2) both installation and removal of glyoxal adducts proceed under mild reaction conditions, (3) glyoxal reactivity towards nucleobases rather than backbone moieties suggests a general approach to cage a variety of different nucleic acid scaffolds including xenonucleic acids (XNAs), (4) glyoxal caging can be performed on both synthetic and naturally occurring nucleic acids, and (5) the reagent itself is both economical and commercially available.

Herein we explore the use of glyoxal for thermoresponsive control over nucleic acid structure and function. We show that glyoxal can effectively cage a wide range of natural and synthetic nucleic acid polymers, providing control over multiple functions including small-molecule binding, catalysis, antisense hybridization, interactions with proteins, and gene expression modulation in cells. Glyoxal caging is efficient and fully thermoresponsive, enabling reduction of function to undetectable levels and full reactivation. Moreover, restoration

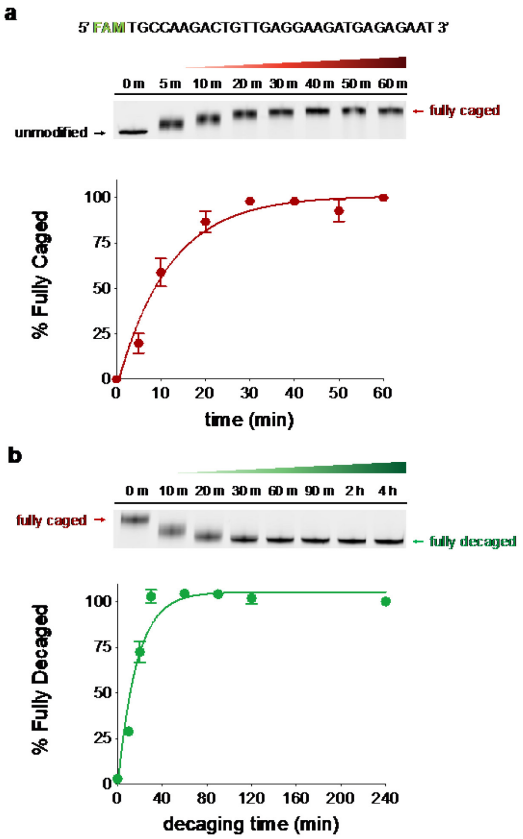

Figure 2. Glyoxal caging and decaging of a DNA substrate. a) Caging kinetics were monitored for a FAM-labeled DNA substrate at 50 ºC using 20% denaturing PAGE. Mean values (n = 2) represent normalized percentages versus band intensity at t = 60 min with S.D. error bars. b) Estimated decaging yield at 95 ºC, pH 7.5 using 20% denaturing PAGE. Values represent mean (n = 2) normalized percentages versus band intensity of an untreated DNA control. Error bars denote S.D.

Table 1. Half-life for glyoxal decaging with varying pH and temperature.

	pH 6.5	pH 7.0	pH 7.5	pH 8.0
95 ºC	1.4 ± 0.34 min	1.1 ± 0.24 min	< 1 min	<< 1 min
70 ºC	52 ± 7.7 min	14 ± 2.7 min	11 ± 2.4 min	3.8 ± 1.6 min
50 ºC	14 ± 1.8 h	8.0 ± 1.7 h	4.6 ± 1.1 h	3.1 ± 0.70 h
37 ºC	14 ± 4.2 d	6.6 ± 1.4 d	3.0 ± 0.5 d	2.0 ± 0.33 d

A fully caged DNA strand was subjected to varying pH values and temperatures, and decaging was monitored by 20% denaturing PAGE and quantified using densitometry (Figs S1-S4). Numbers denote calculated mean $t_{1/2}$ values (n = 2) with 95% confidence intervals. Values at pH 7.5 and 8.0 for 95 ºC were not calculated due to very short observed decaging times.

of function is tunable by temperature, pH, incubation time, and degree of caging. Together, this research addresses a significant gap in nucleic acid technology by providing a simple and effective way to impart thermoresponsive control over both chemically synthesized and enzymatically generated nucleic acids. Additionally, glyoxal caging is applicable in virtually any nucleic acid scaffold, offering a versatile methodology for designing and implementing stimuli-responsive biomaterials with user-defined chemical architectures.

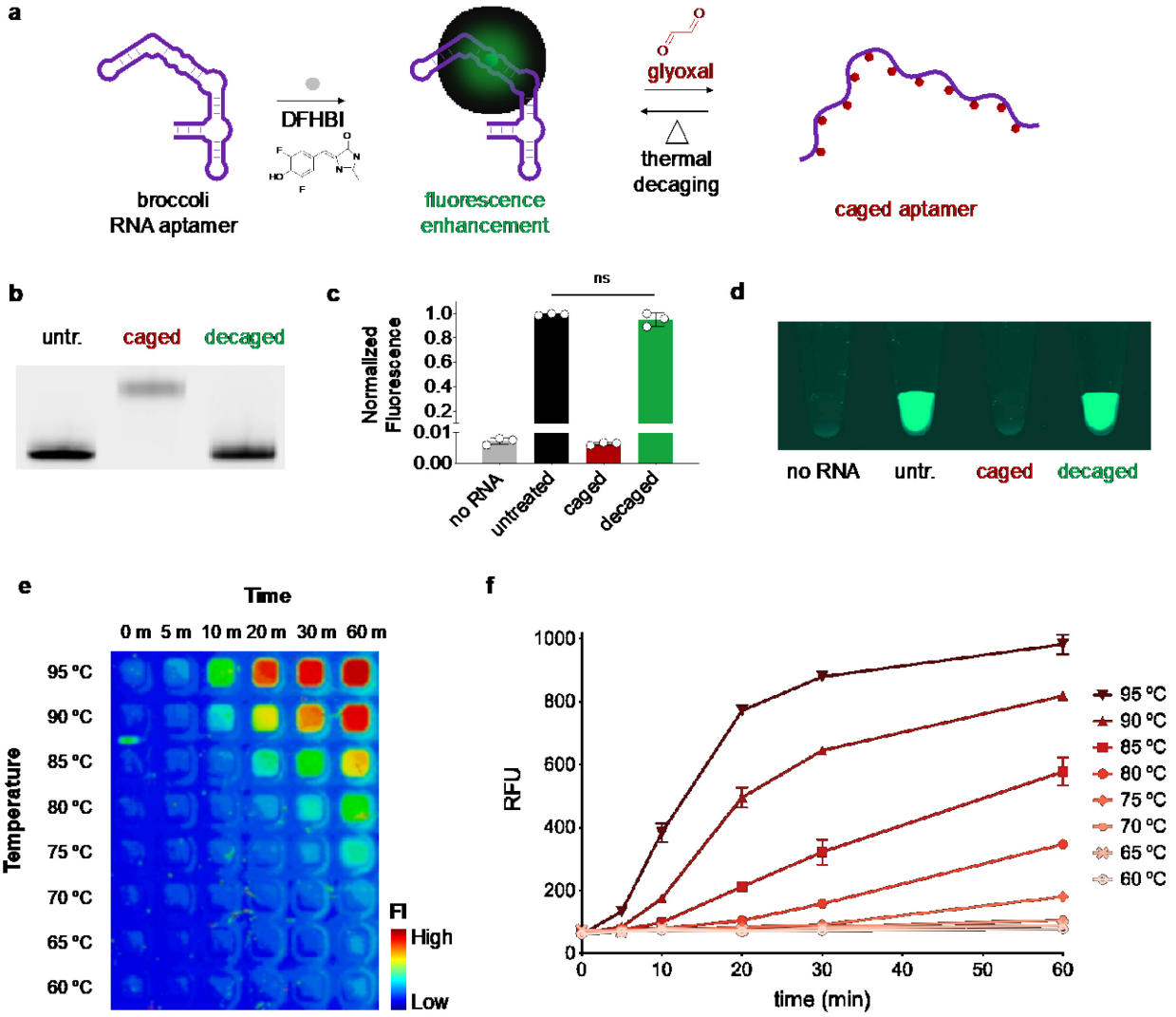

Figure 3. Glyoxal caging imparts thermoresponsive fluorogenic activity in the broccoli RNA aptamer. a) Schematic of the fluorogenic broccoli RNA aptamer. Glyoxal caging reversibly denatures and cages the aptamer, preventing fluorescent signal generation. b) 20% denaturing PAGE analysis of untreated, caged, and decaged RNA aptamers. c) Quantified fluorescence enhancement of untreated, caged, and decaged broccoli aptamers. Bars represent mean and S.D. from triplicate binding reactions. Unpaired t-test was performed between untreated and decaged samples. "ns" indicates no significant difference. d) Fluorescence enhancement reactions visualized with a typhoon gel imager. e) Minimally caged broccoli was combined with DFHBI and incubated at various temperatures for increasing times. Reactions in 384-well plates are visualized using a Typhoon gel imager. Heat map values represent fluorescent intensity generated using the acquisition software (FI = fluorescent intensity). f) Quantified fluorescence plotted against temperature and incubation time. Values represent mean and S.D. of 2 independent trials.

Results and Discussion

Characterizing glyoxal caging and decaging kinetics. We first sought to estimate glycation kinetics in a simple DNA sequence (Figure 2a). Using previously established reaction conditions (1.3 M glyoxal in 50:50 DMSO:H_2O, 50 ºC)[28-29] we monitored molecular weight of our test strand using 20% denaturing PAGE and observed apparent full caging in as little as 30-40 minutes with an approximate $t_{1/2}$ of ~9 minutes (Figure 2a). We were next interested in defining conditions for removing these glyoxal groups, so we first exposed a fully caged strand to standard deprotection conditions (phosphate buffered saline pH 7.5, 70 °C)[29] and again monitored molecular weight shifts as a function of time. As shown in Figure 2b, we observed rapid removal of these groups with apparent full decaging in 30 minutes ($t_{1/2}$ ~11 minutes). We next explored the effect of both pH and temperature parameters in a larger screen and estimated decaging half-life across these conditions (Table 1, Figures S1-S4). In these experiments, we observed that decaging rates were positively correlated to both pH and temperature. Excitingly, this provides a tunable deprotection rate in a variety of assay conditions and highlights the potential of glyoxal caging for constructing programmable nucleic acid-based clocks, thermometers, and pH responsive elements in nanodevices and biological circuits.[30-37] We also assessed room temperature stability of glyoxal adducts and observed minimal decaging over several days, indicating that glycation is stable in practical laboratory conditions until deprotection is triggered by elevated temperatures at the desired time (Figure S5). Although these PAGE experiments provide only a qualitative analysis our model DNA strand, they also illustrate a general kinetic framework of glyoxal caging and decaging. Together, these results demonstrated that glyoxal cage installation and removal were thermoreversible and tunable, and we turned to testing modulation of a wide range of functional nucleic acids.

Thermoreversible modulation of a fluorogenic RNA aptamer. As an initial target to functionally test our method, we selected the "broccoli" aptamer, a well-characterized fluorogenic RNA that binds the small molecule chromophore 3,5-difluoro-4-hydroxybenzylidene imidazolinone (DFHBI) to produce a fluorescent signal (Figure 3a).[38] We hypothesized that only partial caging would be sufficient to disrupt RNA folding and fluorogenic activity, so we first subjected the aptamer to increasing caging times and functionally tested the fluorescence. We observed that only ~5 minutes of caging time reduced activity by > 98%, with complete loss of fluorescence at 10 minutes (Figure S6). While additional reaction times produced proportional increases in molecular weight corresponding to further glyoxalation (Figure S6a), these alterations provided no added functional benefit. Interestingly, we also noted that increased glycation resulted in proportional losses in SYBR Gold staining intensity, further highlighting potent disruption of nucleic acid and small molecule interactions. We utilized our minimal caging time (10 minutes) and subjected these constructs to rapid decaging conditions at 95 ºC, pH 7.5 with increasing reaction times (Figure S7). As expected, we observed a quick rise in signal from 0-2 minutes, and achieved complete restoration of fluorogenic activity after 2 minutes of decaging. We also observed a rapid drop in fluorescence enhancement with extended incubation times, which is likely due to base-mediated RNA hydrolysis at high temperatures, consistent with previously observed degradation of riboswitches in similar buffer conditions at extended heating times.[39] Using our optimized conditions (10 minutes glyoxal caging, 2 minutes decaging at 95 ºC, pH 7.5) we demonstrated both a full masking and complete restoration of broccoli fluorescence enhancement using glyoxal caging (Figures 3b-d). Together, these data demonstrate that glyoxalation is a rapid, potent, and fully reversible method to inhibit small molecule binding in aptamers, and is comparable to current caging methods which achieve similar modulation of activity.[15-16]

Given the simple fluorescent readout of the broccoli system along with our previous characterizations showing tunable thermal decaging kinetics, we next tested our ability to deprotect glyoxal adducts *in situ* for use as a one-pot molecular "thermometer" or "clock". We combined minimally caged broccoli (10 minutes) with all necessary fluorogenic components (2 µM DFHBI, 40 mM HEPES, 100 mM KCl, 1 mM $MgCl_2$, pH 7.4), and then exposed these mixtures to a range of temperatures for increasing times. As shown in Figures 3e-f, we observed a highly predictable and proportional fluorogenic response to both of these variables, with optimal temporal linearity between ~80 ºC and ~85 ºC, and the most proportional thermal response following 60 minute incubation times. Overall, these results highlight the applicability of glyoxal-caged fluorogenic aptamers in designing molecular components in synthetic biology, including nucleic acid-based thermometers and timers. Further, these conditions are generalizable and can yield predictable changes in activity, allowing users to adjust the speed and intensity of responses by altering temperature, aptamer caging time, and/or buffer pH.

Reversible caging of a DNAzyme catalyst. Encouraged by these results, we next sought to control the activity of a catalytic nucleic acid and chose a DNAzyme to demonstrate the versatility of our method across different nucleic acid backbones. Specifically, we employed the 10-23 DNAzyme which hybridizes to a ssDNA target and cleaves at an internal ribonucleotide (Figure 4a).[40] We first assessed caging kinetics

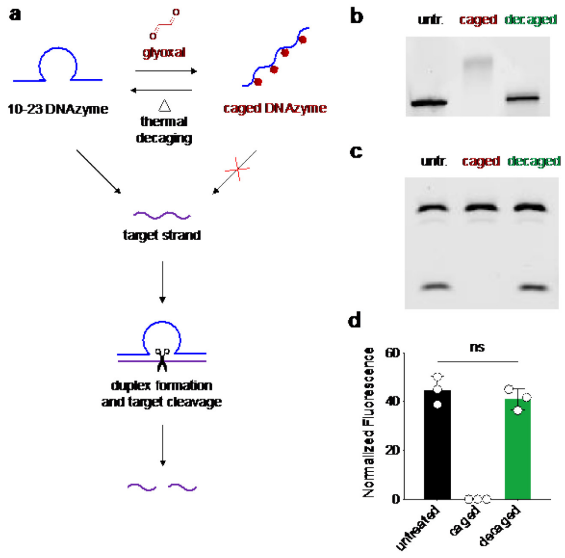

Figure 4. Reversible control of the RNA-cleaving 10-23 DNAzyme. a) Schematic of the 10-23 DNAzyme-mediated cleavage of the target strand following hybridization. Glyoxal reversibly inhibits hybridization and catalytic activity. b) 20% denaturing PAGE analysis of untreated, caged, and decaged 10-23 DNAzyme. c,d) Functional activity of untreated, caged, and decaged 10-23 DNAzyme was monitored as percent target strand cleavage (n = 2) using 12% denaturing PAGE and quantified using band densitometry. Values represent mean and S.D. of 2 independent trials. Unpaired t-test was performed between untreated and decaged samples. "ns" indicates no significant difference.

of the 10-23 strand, observing expected increases in apparent size by denaturing PAGE (Figure S8a). We then tested the functional activity of increasingly caged DNAzyme samples and saw that target cleavage was significantly reduced after 20 minutes of caging, and completely ablated after 1 hour (Figure S8b,c). As expected, this structural shift was also reversible, and when we employed rapid decaging conditions (95 °C, pH 7.5) we observed restoration of the original size after 10 minutes (Figure S9). Using these parameters (20 minutes caging, 10 minutes decaging), we then demonstrated full reversibility of DNAzyme activity (Figures 4b-d). Untreated 10-23 DNAzyme cleaved ~45% of the target strand, whereas caged DNAzyme had no detectable activity. However, this activity was restored upon thermal decaging and displayed ~41% target cleavage with no significant difference compared to untreated DNAzyme. These results demonstrate that glyoxal caging is applicable to DNA substrates and can reversibly modulate catalytic cleavage activity. Moreover, we achieve comparable performance to alternative caging methods that require significantly more expensive reagents.[15-16, 41-42]

Glyoxal caging enables thermoreversible control of modified nucleic acids. After demonstrating reversible control of RNA and DNA constructs, we next sought to explore glyoxal caging of non-native XNA nucleic acid scaffolds. To test this, we first selected the ARC259 RNA aptamer targeting vascular endothelial growth factor (VEGF) (Figure 5a).[43] This particular aptamer was evolved using a fully 2′-*O*-methylated library and would enable us to not only assess disruption of aptamer-protein binding interactions, but also glyoxal caging on a heavily modified scaffold. We first verified that caging kinetics were similar with the ARC259 aptamer, and again saw a predictable rise in apparent molecular weight with increasing glyoxal caging times (Figure S10a). Next, we utilized

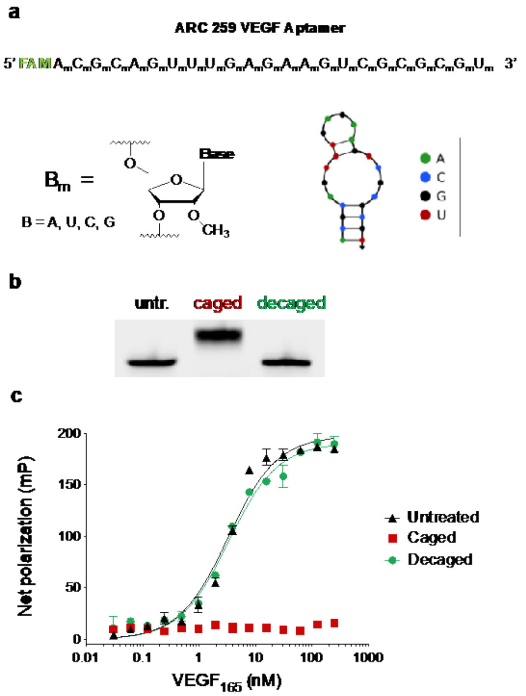

Figure 5. Glyoxal caging of a fully 2'-*O*-methylated RNA aptamer. a) Sequence and NUPACK[44] fold analysis of 2'-*O*-methylated ARC259 RNA aptamer. b) 20% PAGE analysis of untreated, caged and decaged ARC259 aptamer. c) Fluorescence polarization (FP) binding curves of untreated, caged, and decaged aptamer towards $VEGF_{165}$. All values were normalized to a buffer blank and represent mean and S.D. of independent replicates (n = 3).

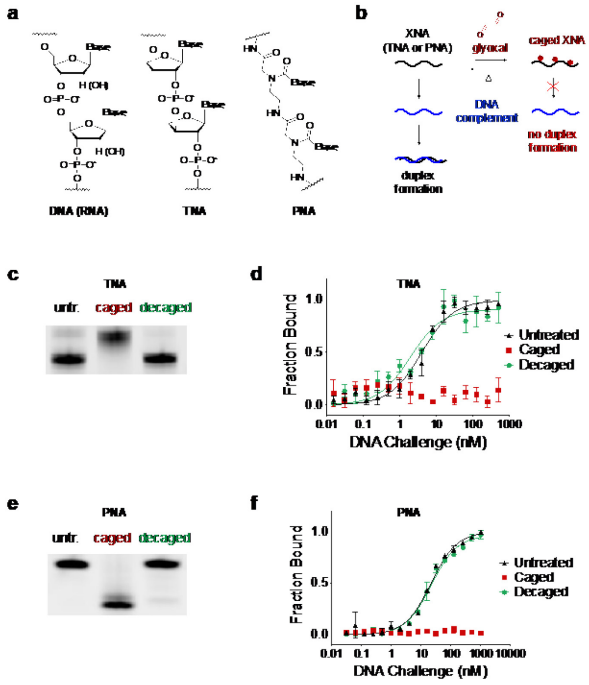

Figure 6. Glyoxal caging reversibly inactivates xenonucleic acid hybridization. a) Chemical structures of DNA/RNA alongside threose nucleic acid (TNA) and peptide nucleic acid (PNA) scaffolds. b) Heteroduplex formation between XNA strands and a DNA complement. Glyoxal caging reversibly inhibits duplex formation. c) 20% denaturing PAGE analysis of untreated, caged, and decaged TNA strands. d) MST binding curves of untreated, caged, and decaged TNA strands when challenged with increasing amounts of DNA complement. Bars represent mean and S.E. from triplicate binding titration curves. e) 20% denaturing PAGE analysis of untreated, caged, and decaged PNA strands. f) MST binding curves of untreated, caged, and decaged PNA strands when challenged with increasing amounts of DNA complement. Bars represent mean and S.E. from triplicate binding titration curves.

fluorescence polarization (FP) to monitor ARC259-VEGF binding. Unsurprisingly, untreated aptamer displayed high affinity towards the target protein, and increasing caging times proportionally decreased this interaction, with ~40 minutes glyoxal treatment resulting in full loss of aptamer binding (Figure S11). We were next interested in restoring this activity, so we then subjected minimally caged ARC259 (40 minutes) to rapid decaging conditions (95 ºC, PBS pH 7.5) and observed a predicted drop in apparent molecular weight in 20% denaturing PAGE with ~2-5 minutes decaging time (Figure S10b). Lastly, we compared the binding activity of untreated, caged, and decaged ARC259 in our FP assay (Figure 5c), and observed nearly identical binding affinities between untreated and decaged aptamers (K_D untreated = 3.27 ±0.59 nM, K_D decaged = 3.36 ±0.55 nM). Together, these results demonstrated the versatility of glyoxal caging towards chemically modified substrates, and further showed reversible control over protein-aptamer interactions. Additionally, to our knowledge, this is the first demonstration of post-synthetic caging of a 2' modified RNA aptamer, which has not been possible with previous cloaking methods that target 2'OH groups.[15-16]

Encouraged by the versatility of our approach, we next wanted to apply glyoxal caging toward non-canonical xenonucleic acid scaffolds. In particular, we targeted threose nucleic acid (TNA) and peptide nucleic acid (PNA). Compared to DNA or RNA, TNA is comprised of repeating threose sugars connected with alternating 2' to 3' phosphodiester bonds,[45] while PNA consists of amino ethyl glycine units to form a "peptide" rather than phosphodiester backbone (Figure 6a).[46] Due to their non-canonical chemical structures, both TNA and PNA are nuclease-resistant and are promising antisense oligonucleotide scaffolds. Additionally, these unique structural features are intriguing for demonstrating the flexibility of glyoxal caging with chemically modified substrates. As shown in Figure S12, we first assessed glyoxal caging kinetics with a model TNA oligonucleotide, and observed nearly identical kinetics compared to DNA. We next evaluated the effect of caging on hybridization between TNA and a DNA complement or scrambled oligonucleotide. We utilized microscale thermophoresis (MST) to measure duplex formation, as this method would preserve caging groups during analysis and has been previously demonstrated as a highly sensitive reporter of nucleic acid hybridization.[47-48] We observed steady disruption of duplex formation with increasing caging times on our TNA strand, with ~40 minutes of glyoxal treatment resulting in full ablation of hybridization capacity (Figure S13). Using these minimal caging conditions (40 minutes), we then used our rapid decaging protocol (5 min at 95 ºC in PBS, pH 7.5) to remove glyoxal adducts from TNA, observing full restoration in duplex formation (Figure 6c,d). To apply these experiments towards PNA, we then synthesized the "Nielsen decamer" sequence as a model strand (Figure S14).[49] Interestingly, when assessing glyoxal caging of PNA, we saw an unexpected drop in apparent molecular weight in 20% denaturing PAGE with increasing caging times (Figure S16a). While we were initially concerned about possible degradation or hydrolysis, we did confirm an increase in mass corresponding to the addition of

two glyoxal caging groups (Figure S15). Additionally, this effect was also reversible, and when we subjected a fully glyoxalated PNA strand to thermal decaging conditions at 95 ºC, pH 7.5, an opposite electrophoretic shift was observed, suggesting full removal of glyoxal groups (Figure S16b). Although uncertain, we hypothesize that glyoxal adducts may impart transient negative charges to the strand through cooperative hydrogen bonding between hydroxyl adducts to produce an ionizable proton (Figure S17). In the case of PNA where the only anion present is a terminal glutamate residue (Figure S14a), these alterations may contribute more significantly to electrophoretic shift than molecular weight changes. These analyses also yielded 3 visibly discrete bands, suggesting that guanosine addition products may be the predominant species in PNA glyoxal caging. When we tested hybridization capacity of increasingly caged PNA, we observed highly potent disruption following glyoxal treatment, observing a significant drop between 5 and 10 minutes caging time, and only 20 minutes required for full inhibition of duplex formation (Figure S18). Finally, we compared untreated, caged, and decaged PNA and again observed full restoration of duplex binding (Figure 6e,f). Together, our results show that glyoxal caging is a straightforward and robust method for reversibly modulating antisense interactions, and to our knowledge is the first demonstration of functional caging in non-canonical nucleic acid substrates.

Glyoxal caging of nucleic acids reversibly modulates interactions with enzymes. Based on our results thus far showing reversible modulation of protein-nucleic acid interactions as well as the known molecular changes imparted by glyoxal addition on nucleobases, we were curious how caging would impact recognition by enzymes that interact with nucleic acid substrates (Table 2). RNase T1 is historically known to be affected by glyoxalation, which cleaves after both guanosine and inosine residues but is unable to digest caged guanosines, resulting in highly specific cleavage activity toward inosine.[28-29] We tested other enzymes starting with RNase H, which cleaves RNA substrates when hybridized to complementary DNA.[50] We first incubated a target RNA strand with or without glyoxal for 1 hour, followed by hybridization to a complementary DNA strand and exposure to RNase H. Untreated heteroduplex was cleaved as expected, while caging of the ssRNA substrate prior to hybridization and digestion resulted in no detectable cleavage. Upon thermal decaging, full restoration of cleavage activity was achieved (Figure S19). Given our previous "one pot" thermoreversible readout using the fluorogenic broccoli RNA aptamer (Figure 3e-f), we were interested in recapitulating similar *in situ* decaging and cleavage using a thermostable RNase H.[51] To test this, we combined caged ssRNA, complementary DNA, and thermostable RNase H in 1X reaction buffer (50 mM Tris-HCl, 75 mM KCl, 3 mM $MgCl_2$, 10 mM DTT, pH 8.3). Reactions were then separately heated to 95 °C for increasing time points, followed by one hour at 37 °C. As shown in Figure S20, we observed a steady and predictable increase in RNase H cleavage activity approaching 100% restoration over 10 minutes, indicative of proportional decaging of the target RNA strand with increased exposure to heat. These results were consistent with our previous "one pot" system measuring fluorogenic activity of the broccoli aptamer (Fig 3e-f), and we predict that both temperature and heat exposure time can be proportionally measured via RNase H cleavage and similarly leveraged towards construction of biological "timers" and "thermometers."

We next evaluated caging on the activity of RNase A, an endonuclease that cleaves single and double stranded RNA after cytidine and uridine nucleotides.[52] However, glyoxal addition was not able to inhibit activity, and distinct cleavage sites were present for all untreated, caged, and decaged RNAs (Figure S21). Similar results were observed with nuclease P1, a broadly active endonuclease that hydrolyzes phosphodiester bonds in 3′ → 5′ direction,[53] and glyoxal caging of ssDNA and ssRNA substrates still resulted in full digestion activity (Figure S22). We next tested DNase I, an endonuclease that preferentially cleaves double-stranded DNA substrates after pyrimidine nucleotides.[54] Similar to our previous experiments, we first treated a target DNA strand with or without glyoxal followed by hybridization to a complementary DNA and exposure to DNase I. As shown in Figure S23, glyoxal caging completely inhibited DNase I activity, and full cleavage of the target strand was observed upon thermal decaging. We observed similar results with the restriction endonuclease EcoRI, with glyoxal treatment reversibly modulating enzymatic cleavage of the target duplex (Figure S24).

Table 2. Glyoxalation reversibly modulates activity in several enzymes.

Name	Type	Target	Inhibition?
RNase T1	Endonuclease	ssRNA after G residues	Partial*
RNase H	Endonuclease	RNA:DNA heteroduplexes	Yes
RNase A	Endonuclease	ssRNA, dsRNA	No
Nuclease P1	Endonuclease	ssRNA, ssDNA	No
DNase I	Endonuclease	ssDNA, dsDNA (preferred)	Yes
EcoRI	Endonuclease	dsDNA at palindromic sequence 5' GAATTC 3'	Yes
RNase T	Exonuclease	3' exonuclease	No
Phosphodiesterase I	Exonuclease	5' exonuclease	No

*glyoxal reacts with G residues but not inosine sites, converting RNase T1 into an inosine-specific endonuclease.[28-29]

Lastly, we were curious as to whether glyoxal interfered with exonuclease activity. We first tested RNase T, a 3'→ 5' exonuclease active on both ssRNA and ssDNA targets.[55-56] Unfortunately, caging exerted no effect on RNase T activity, and full hydrolysis of DNA and RNA substrates was observed regardless of glyoxal caging (Figure S25). Similar results were obtained when testing snake venom phosphodiesterase I which hydrolyzes ssDNA and ssRNA in the opposite 5' → 3' direction,[57] and glyoxal caging offered no protection toward enzymatic degradation of either DNA or RNA strand (Figure S26). While disappointing, these results are also somewhat unsurprising given that exonuclease sequence specificity is known to be broad and inherently promiscuous, and these enzymes interact primarily with the phosphate backbone irrespective of nucleobase or modification status.

As compiled in Table 2, it was apparent that glyoxal caging was most effective where nucleic acid secondary structure was required for substrate engagement and activity. In particular,

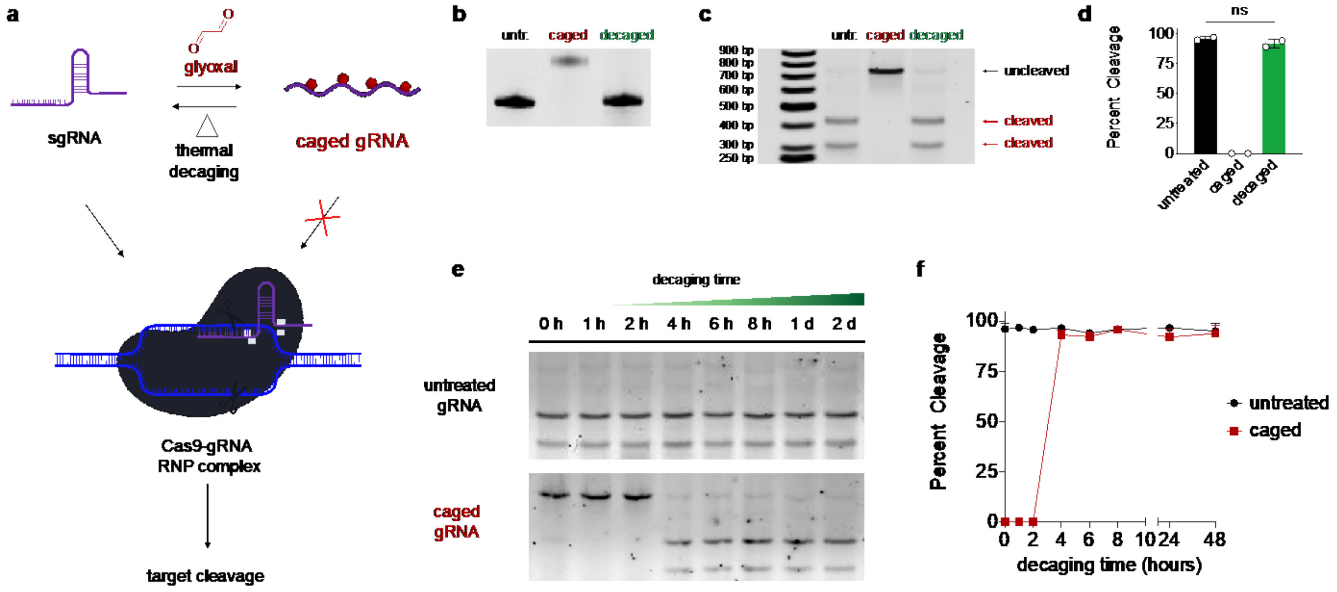

Figure 7. Thermal reactivation of CRISPR-Cas9 function. a) Schematic of reversible modulation of CRISPR-Cas9 cleavage. Glyoxal caging reversibly denatures and cages the sgRNA, preventing RNP complex formation and target cleavage. b) 20% denaturing PAGE analysis of untreated, caged, and decaged sgRNAs. c) Functional Cas9 target cleavage with untreated, caged, and decaged sgRNAs visualized by 1% agarose gel and d) quantified using densitometry. Bars represent mean and S.D. from 2 independent trials. Unpaired t-test was performed between untreated and decaged samples. "ns" indicates no significant difference. e) Caged sgRNAs were decaged at 37 ºC for increasing times and combined with Cas9 and dsDNA target followed by 1% agarose gel analysis and f) quantified using densitometry. Values represent mean and S.D. of 2 independent trials.

RNase H, DNase I, and EcoRI all preferentially target duplex substrates, and glyoxal inhibition can be mechanistically attributed toward preventing hybridization and subsequent presentation of preferred substrates. With the exception of RNase T1, all other enzymes tested appeared to have little sensitivity to glyoxal, as these likely prefer single stranded substrates and potentially act independent of nucleobase structure. Overall, our screen yielded distinct enzyme candidates that could be leveraged to produce detectable readouts, and further demonstrates the wider versatility of glyoxal caging towards thermoresponsive biodevice fabrication.

Thermal reactivation of CRISPR-Cas9 using glyoxal caged guide RNAs. Based on our survey of reversible enzyme disruption using glyoxal caged substrates, we hypothesized that we could likely modulate CRISPR-Cas9 activity. In this system, a single guide RNA (sgRNA) acts as both an aptamer towards Cas9 to bind the nuclease as well as a programmable sequence-specific probe to bring the ribonucleoprotein (RNP) complex to a desired genetic locus for cleavage (Figure 7a).[58-59] These platforms have proved to be revolutionary towards perturbing biological circuits and have great promise in human gene therapy. As such, there is great interest in exerting tunable external control over CRISPR-based systems. Similar to previously described nucleic acid caging approaches, existing attempts have primarily focused chemical or light-based activation of sgRNAs.[60-62] However, heat activation of sgRNA again remains uninvestigated, and we predicted that glyoxal caging would provide a facile approach for imparting predictable thermal and temporal control. We envisioned that glyoxal cages would denature sgRNA secondary structure required for RNP complex formation while also strongly inhibiting base-pairing at the DNA-gRNA interface, thus ablating Cas9 activity. We first determined the minimal degree of caging required for shutdown of Cas9 cleavage of a 720 bp dsDNA target containing an enhanced green fluorescent protein (eGFP) coding region.[63] In contrast to the steady drop in activity with increasing caging times as seen in our previous experiments, we interestingly saw minimal inhibition of activity over 30 minutes of glyoxal caging followed by a drastic drop in cleavage after ~40 min–1 hour, and a full 2 hours of caging was necessary to completely shut down Cas9 activity (Figure S27). We hypothesize that this higher resistance to caging may be due in part to the uridine-rich nucleotide sequence of CRISPR sgRNAs, as these bases are not known to react with glyoxal.[18-22] Given our previous experiments with both broccoli and ARC259 RNA aptamers, it is also likely that partially caged sgRNAs are still functionally active with Cas9, which would explain maintenance of cleavage activity despite observed sgRNA caging via PAGE (Figure S27a). In our studies we utilized a commercially available Cas9 enzyme from *Streptococcus Pyogenes* which is known to exhibit single-turnover kinetics,[64] and so it is unlikely that individual RNP complexes would cleave multiple DNA targets. However, we did employ a moderate excess (~6-7-fold) of Cas9/sgRNA complex compared to DNA target, so these reaction conditions may have also contributed to our observed results. Glyoxal caging was nonetheless effective in completely inhibiting Cas9 cleavage, and so we next sought to thermally restore this activity. We first subjected caged sgRNAs to our rapid decaging conditions at 95 ºC, pH 7.5, and when we combined these with Cas9 enzyme and dsDNA target, full activity was restored with 2 min of decaging time (Figure S28). These data also reflected our caging observations in that Cas9 activity did not steadily increase with decaging times but rather rapidly increased between 0.5-2 min. Additionally, our results corroborate our earlier notion that partially caged sgRNAs still promote Cas9 activity, as full cleavage was still observed from 2-10 min (Figure S28b) despite our PAGE shift analysis suggesting full decaging occurring at ~ 5 mins (Figure S28a). Regardless, when compared to untreated sgRNA there was also no significant difference in Cas9

cleavage activity when paired with a decaged sgRNA (Figure 7b-d), overall demonstrating that glyoxal caging is a fully reversible method of controlling CRISPR-Cas9 function.

Given the practical use of CRISPR-Cas9 systems for *in vivo* gene editing applications, we were curious to see if we could replicate thermal reactivation of Cas9 activity under "physiological" conditions. To explore this, we incubated caged sgRNA at 37 °C in PBS, pH 7.5 for increasing periods of time. We first assessed size shift by gel, which expectedly decreased over 2 days (Figure S29). We also tested each timepoint for functional Cas9 cleavage activity against an untreated sgRNA control, and we observed full restoration after 4 hours at 37 °C (Figure 7e,f). Together, these results demonstrate the feasibility of our approach for caging and thermally reactivating CRISPR-Cas9 systems for potential use in biological circuits, nanodevices, and *in vivo* applications. Additionally, in our proof-of-concept demonstration we used a standard DNA cleavage readout. However, this is only one application of this platform, and glyoxal caging can likely also be used in applications such as gene activation,[65] gene interference,[66] base editing,[67] or prime editing,[68] which rely on dead Cas9 fusions. In addition, designer systems have been developed that combine guide RNA targeting with fully human effector protein components,[69] and we envision the use of glyoxal caging as a useful and straightforward method for tuning activity in these systems.

Glyoxal treatment of DNA primers enhances PCR specificity. Polymerase chain reaction (PCR) is a widely adopted molecular biology technique and a powerful diagnostic method for quantifying gene expression[70] and detecting genetic material.[71] While highly sensitive and efficient, PCR is also prone to non-specific amplification of off-target DNA products. Many of these issues arise from undesired molecular interactions, including primer-dimer formation and non-specific annealing within DNA templates, which primarily occur during lower-temperature steps in early PCR rounds.[72] To mitigate these effects, "hot start" PCR assays are often employed wherein DNA polymerase is inactivated with aptamers and/or antibodies to prevent primer extension until high temperatures are reached.[73-74] While this technique can reduce some PCR artifacts, hot start polymerases are also variably effective for primer-dimers and off-target products, and the added cost of these neutralizing biocomponents can be prohibitive for some applications. Alternatively, primers can be chemically modified with photoactivatable[75] or thermolabile[76] adducts to provide similar improvements in PCR performance. Although these modifications are more effective for directly addressing issues with mis-priming, these methods also suffer from similar practical limitations described above, as they necessitate costly incorporation of chemical groups during solid-phase oligonucleotide synthesis and typically require extensive optimization. Conversely, glyoxalation is cost-effective, tunable, and can be applied toward a variety of modified nucleic acid scaffolds, and hence may offer greater applicability in improving PCR performance. Because glyoxal adducts potently disrupt nucleic acid hybridization and are fully reversible using heat, we were interested to see if this method would prevent off-target primer interactions and improve overall amplification specificity (Figure 8a).

As a model system, we amplified a ~653 bp segment of the β-actin gene (*ACTB*) using human total DNA and a standard *Thermus aquaticus* (*Taq*) polymerase, a combination which was found to be prone to both mis-priming and primer-dimers.[76] Additionally, a previous study attempted chemical modification of DNA primers and found this mildly improved PCR performance, and we were interested to see if glyoxalated primers would be better suited for addressing mis-priming issues in PCR (Figure 8a). We first attempted amplification using standard *Taq* PCR reagents, and while we observed the expected target band, we also experienced general "smearing" in reactions as well as the presence of an off-target amplification product at ~400 bp. Additionally, in the absence of any DNA template, products arising from primer-dimer formation were identified at ~150 bp (Figure S30a). Given that antibody-neutralized hot start *Taq* is commonly employed to mitigate these issues, we repeated this experiment using these materials, and while we saw a slight reduction in the formation of off-target products, this ultimately provided little benefit in overall amplification purity (Figure S30a,b). We next functionally assessed glyoxal treatment by separately caging either the forward or reverse DNA primer. Interestingly, treating the forward primer produced almost no effect (Figure S31), and although reverse primer caging did somewhat

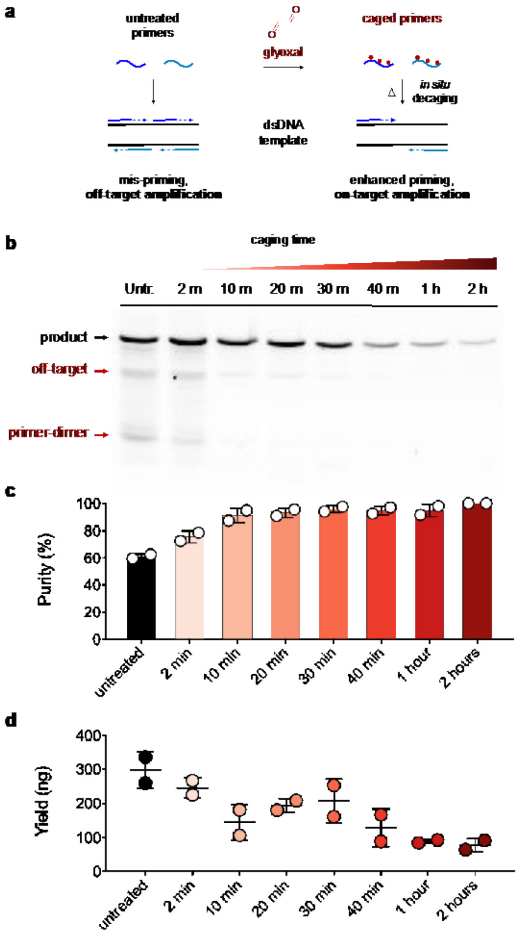

Figure 8. Glyoxal treated primers enhance PCR specificity. a) Schematic of PCR amplification using a dsDNA template with untreated and caged primers, which reduce mis-priming and primer-dimers. b) 1% agarose gel analysis of PCR reactions to generate a 653 bp *ACTB* product from human genomic DNA with untreated and increasingly caged primers. c) Densitometric quantification of on-target PCR amplification purity with caged primers. Bars represent mean and S.D. from 2 independent trials. d) Overall PCR yield following amplification and purification. Bars represent mean and S.D. from 2 independent trials.

enhance amplification specificity (~60% to ~85%), we were disappointed that only moderate improvements were observed for all caging timepoints tested (Figure S32). Surprisingly, when we caged both primers prior to PCR, we saw a significant improvement in amplification specificity (Figure 8b,c). This effect was particularly evident between 0-10 minutes glyoxal treatment time, where observed purity values increased from ~60% to >90%. Moreover, extended primer caging times beyond 30-60 minutes resulted in PCR yields approaching >95% purity. Importantly, glyoxal caging almost completely eliminated both off-target amplification and primer-dimer issues (Figure 8b), and outperformed previous attempts using thermolabile chemical adducts, which did not suppress these artifacts in the same system.[76] We hypothesized that this enhancement was due to a slow, iterative release of active primer throughout PCR cycles. To verify this, we glyoxalated both primers for 10 minutes and then monitored primer decaging in our reaction buffer (10 mM Tris-HCl, 50 mM KCl, 1.5 mM $MgCl_2$, pH 8.3) during the initial denaturation step and subsequent PCR cycles. Interestingly, full decaging of primers was not observed until cycle 20 as monitored by denaturing PAGE shift (Figure S33), supporting the idea that stoichiometric limiting of available active primer may contribute to enhanced specificity. We highlight that our glyoxal system is the first to be able to achieve this type of time-released activation of primers across multiple PCR cycles. We also quantified total dsDNA yields after purifying each PCR reaction, and although this led to an expected proportional drop in recovered product, this comes with the large benefit of significantly increased purity (Figure 8c,d). Primer concentration is often the limiting reagent for total amplification yield, and given our analysis of primer decaging, it is likely that very long caging times result in a proportion of primers that remain caged throughout the entire thermal cycling program. A larger number of cycles would likely activate these remaining caged primers and may improve yields. Overall, our results demonstrated that glyoxal is a straightforward and tunable modification for enhancing PCR amplification specificity, and will likely benefit both standard molecular biology assays as well as high-accuracy PCR-based diagnostics.

Time-release thermal reactivation of a caged antisense oligonucleotide in human cells. After exploring a wide range of *in vitro* applications, we were interested in demonstrating the ability of glyoxal-caged nucleic acids to modulate function in a cellular environment. Because glyoxal disrupts Watson-Crick-Franklin base pairing, we hypothesized that an antisense oligonucleotide (ASO) would be strongly affected by caging and that we could reversibly modulate its overall function. Titratable gene interference is also emerging as a powerful strategy for profiling cellular proteomes and engineering metabolic pathways,[77-78] and we were curious if a glyoxal-caged ASO would allow us to exert tunable and predictable control over gene expression in living cells. To test this idea, we identified a chemically modified "gapmer" ASO optimized to silence eGFP expression by targeting and degrading its cognate mRNA via the canonical RNase H-mediated decay pathway (Figure 9a).[79-80] This ASO class is comprised of locked-nucleic acid (LNA) nucleotides at each terminus and contains phosphorothioate linkages throughout the strand, endowing these molecules with high endonuclease resistance and biostability while retaining functional compatibility with cellular gene silencing machinery.[81-83] Using this system, we reasoned that glyoxal caging would temporarily inhibit the ability of the ASO to hybridize to its target mRNA, thus blocking gene suppression activity (Figure 9b). Based on our previous kinetic analyses for decaging RNA constructs at 37 ºC (Table 1 and Figure 7e), we also hypothesized that this activity could be restored to shut down GFP synthesis in a predictable and tunable manner. Although a widely-adopted and useful fluorescent reporter, GFP also displays remarkable stability ($t_{1/2}$ ~26 h) and accumulates at high levels in the cytoplasm,[84] which can interfere with detecting transient changes in mRNA levels. To circumvent this, GFP is often destabilized by appending a proteolytic "degron" sequence to promote rapid turnover and facilitate temporal detection of transcriptional activity.[85-86] We were concerned that high GFP stability would mask our ability detect ASO function and reactivation, and so to avoid this outcome and enable high-resolution tracking of mRNA degradation in real-time, we appended a similar C-terminal degron tag (supplemental methods).

After inserting this construct into a cytomegalovirus (CMV) mammalian expression plasmid, we first confirmed reasonable transfection efficiency and GFP expression in HEK293T cells by fluorescence microscopy (Figure S34). We next wanted to identify an optimal ASO concentration sufficient for silencing GFP expression, as well as validate the specificity of this previously tested sequence.[79] As shown in Figure S35, cells treated with ~250-500 nM of a GFP-targeting ASO exhibited virtually no detectable GFP signal, while a scrambled sequence produced no GFP inhibition across all concentrations tested, indicating potent ASO-mediated silencing of GFP synthesis in a sequence-specific manner. Using these optimal conditions (250 nM ASO) we next created a library of increasingly caged ASO samples, and assessed the impact of glyoxal caging on GFP silencing by co-transfecting HEK293T cells with both the pCMV-GFP vector and respective ASOs. We then imaged all cells after a 12 h recovery period and interestingly saw that ~6-8 h glyoxal treatment time was necessary to completely ablate ASO function and produce GFP signal commensurate with cells receiving only plasmid (Figure S37). This treatment time was unexpectedly long compared to some of our previous applications, and while it is possible that some decaging occurs within the 12 h window between transfection and imaging, we also hypothesize that RNase H may tolerate partially caged ASOs, consistent with previous observations that DNA:RNA heteroduplex regions as short as ~4 bp are sufficient for RNA cleavage.[87-89] Ultimately, we were still able to completely inhibit ASO function with glyoxal caging. We were also initially concerned that glyoxalation may simply prevent ASO strands from entering cells, and so we separately exposed HEK293T cells to Cy5-labeled ASOs either unmodified or treated with glyoxal (8 h). As shown in Figure S38, we observed similar internalized fluorescent signal in both untreated and fully glyoxalated samples, and our overall results were consistent with previous studies using these ASO constructs.[79] Combined with our functional results demonstrating GFP silencing in transfected cells, it is likely that caging exerts minimal effect on cellular uptake.

We were next interested in restoring ASO activity *in cellulo*, and so we performed a time-course experiment to monitor GFP expression in HEK293T cells. On day 0, cells received either 1) GFP plasmid alone, 2) plasmid and a fully caged ASO (8 h glyoxal treatment time), or 3) plasmid and an untreated active ASO (Figure 9c). We periodically imaged these samples over the course of 7 days and then used ImageJ[90] to quantify and plot GFP-positive cells in images across groups.

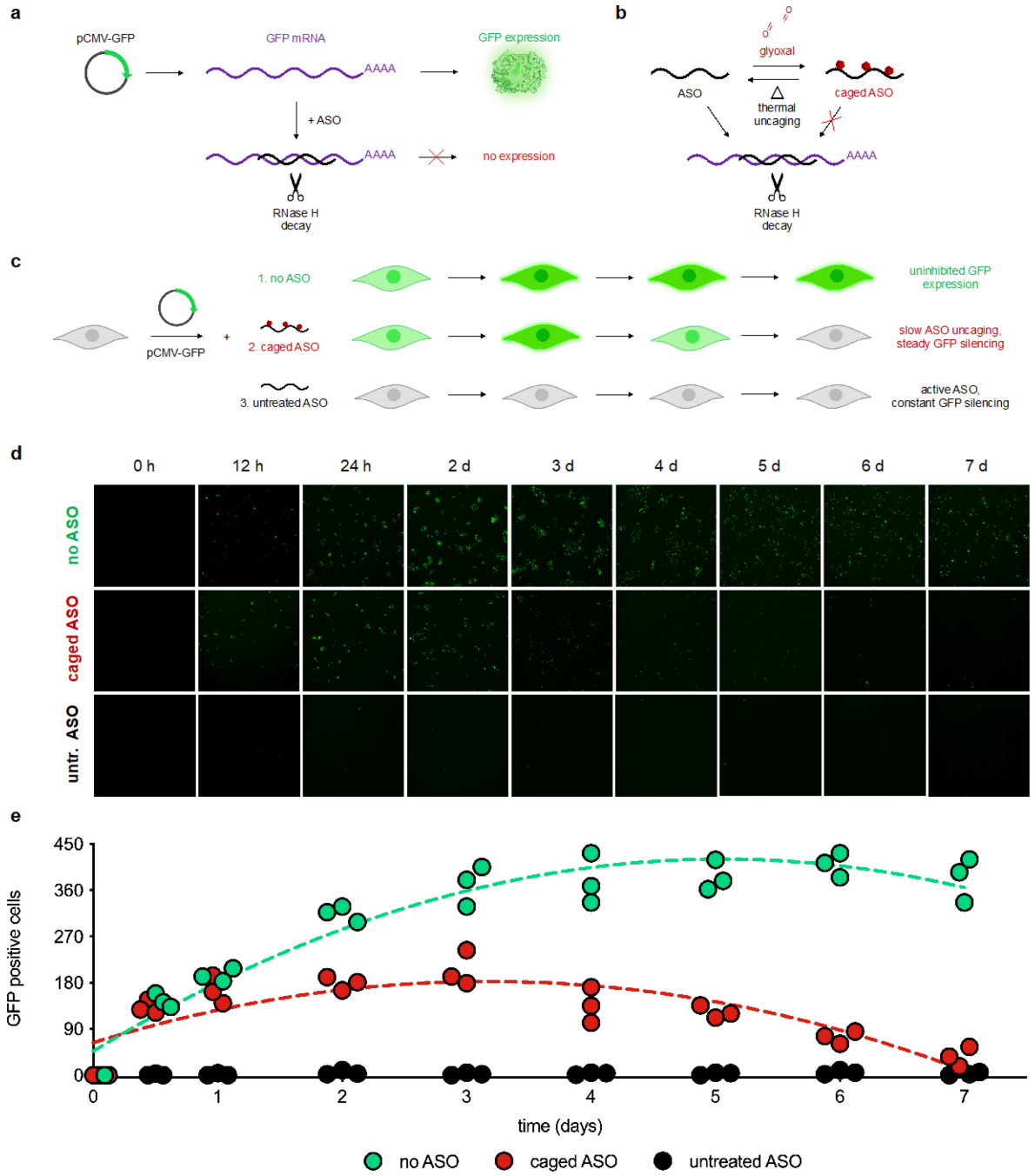

Figure 9. Thermal reactivation of antisense oligonucleotide (ASO) function *in cellulo*. a) Schematic of ASO gene silencing mechanism through antisense mRNA hybridization and RNase H-mediated decay. b) Glyoxal caging reversibly blocks ASO hybridization, preventing silencing complex formation and target cleavage. c) Experimental workflow for *in cellulo* time-release ASO decaging. At $t = 0$, HEK293T cells were transfected with a pCMV-GFP plasmid as well as 250 nM glyoxal caged ASO (red), untreated ASO (black) or no ASO (green). Cells receiving no ASO exhibit uninhibited GFP expression throughout the experiment, while cells given untreated ASO produce no detectable GFP due to constant gene silencing. Cells treated with caged ASO exhibit initial increase in fluorescence due to GFP expression followed by a delayed suppression of GFP signal due to time-release reactivation of glyoxalated ASO. d) Representative live-cell fluorescence microscopy images (4X magnification) taken throughout the course of the experiment. e) Quantification of GFP-positive cells in each field across treatment groups during the experimental time course. Circles represent individual wells (n = 3) from a 96-well plate. Curves are overlayed with a second-order polynomial fit (dashed lines).

(Figure 9d,e). Cells receiving a fully caged ASO exhibited similar increases in GFP expression throughout the first 24 h of the experiment compared to cells receiving only plasmid, suggesting full glyoxal inhibition of ASO function during this period. However, in contrast to control cells which exhibited an increased GFP-positive population and sustained expression throughout days 2-7, cells treated with a caged ASO displayed a steady decrease in GFP-positive cells for the remainder of the time-course experiment, indicating ASO thermal uncaging and reactivation of gene silencing function, with approximately ~90% restoration in function by day 7 (Figure 9d,e). Conversely, cells receiving an un-

treated ASO displayed virtually no GFP expression for the entirety of the experiment, confirming that this ASO concentration (250 nM) was sufficient for gene silencing in proliferating cells across all timepoints. To provide a comparison of decaging in these conditions, we also prepared several caged (8 h treatment time) ASO samples in complete DMEM and monitored decaging at 37 ºC using denaturing PAGE (Figure S39). Interestingly, these data suggest that full ASO decaging may be complete in ~1-2 days, which was somewhat faster than both our previous kinetic analysis on a model DNA strand (Table 1) as well as our functional gene silencing results (Figure 9d,e). To recapitulate *in cellulo* caging conditions, the amount of nucleic acid present in each decaging reaction (250 nM, 1.3 ng/μL) was lower than these previous tests (400 nM, ~4 ng/μL), suggesting that the concentration of caged construct may be an important consideration for thermoreversibility. Additionally, there may also be a "buffer effect" (complete DMEM vs PBS) that could alter the overall kinetics of glyoxal release. While still somewhat faster than our functional *in cellulo* results, these reactions are also a simple representation of a cellular context and we hypothesize that ASO decaging is likely influenced by intracellular pH gradients, which can range from pH 4.5-8 across organelle compartments.[91-92] Moreover, the process of ASO uptake, cytosolic partitioning, and RNA silencing complex formation is a multiphase process with its own kinetics, and additionally competes with multiple cell divisions that can dilute these materials. Ultimately, these PAGE data provide a rough kinetic estimate for decaging and importantly illustrate analytical confirmation that decaging occurs in these conditions (Figure S39).

In nearly all of our previously explored *in vitro* applications, glyoxal treatment time was an adjustable variable to produce proportional decreases in nucleic acid activity, and we were interested if we could similarly tune GFP expression by varying the degree of ASO caging. In parallel with our kinetic analysis using a fully caged ASO *in cellulo,* we also monitored functional gene silencing activity of HEK293T cells co-transfected with both GFP plasmid and increasingly caged ASOs (5 min–8 h glyoxal treatment time). Interestingly, when combined with our previous data, the degree of glyoxal caging in different ASO samples produced a clear correlation in the number of GFP-positive cells in each well, demonstrating that glyoxalation is a feasible method for tuning protein expression levels within cell populations (Figures S40, S41). ASOs treated with glyoxal for 0–30 minutes produced minimal inhibition, while 1-8 hours resulted in relative increases in GFP expression. Additionally, these samples all displayed proportional reactivation of gene silencing activity across 7 days, demonstrating the use of this method to both delay gene suppression as well as modulate overall protein synthesis levels. Although we did not observe full restoration of ASO activity across all caging treatment times (Figures 9e, S40), this would likely be seen in longer decaging experiments past 7 days. We also performed these experiments using highly proliferative immortalized cells (HEK293T), and the predictable reactivation we observed over several days invites interesting use of these constructs to modulate gene expression levels in both terminally differentiated and/or primary cells.

Although a natural cellular metabolite produced from both sugar and lipid oxidation,[93-95] glyoxal can be cytotoxic at higher concentrations,[96-97] and we wanted to verify that slow intracellular release of small amounts glyoxal was tolerable *in cellulo*. Qualitatively, we observed no differences in morphology or growth rate between any cell groups receiving differentially caged ASOs, and all treated cells displayed roughly equivalent doubling times and were confluent by end of the experiment (Figures S40). At the conclusion of day 7, we also tested viability and mitochondrial function of treated cells using a water-soluble tetrazolium assay,[98] and we observed that all ASOs, regardless of degree of caging, produced no significant decreases in viability (Figure S41). In parallel, we also evaluated glyoxal alone in a dose-response viability assay, and did confirm that the reagent itself is cytotoxic, albeit at much higher concentrations (IC_{50} = 310±83 μM, Figure S42). In our example ASO, even if all nucleobase positions contained a glyoxal adduct (16 nt), glyoxal levels would be ~4 μM, well below the concentration where adverse effects are observed. Additionally, the slow release of glyoxal may enable it to be cleared by existing cellular metabolism pathways. Careful monitoring of potential toxicity would obviously be wise when applying glyoxal-modified nucleic acids in pharmaceutical formulations, but in our experiments we saw no observable cytotoxicity from our caged ASOs, demonstrating their compatibility and utility to perturb gene expression in cell populations. Additionally, glyoxal-caged nucleic acid constructs are generalizable, and thus can be used broadly for kinetically tuning gene expression to better understand cellular signaling mechanisms as well as engineer metabolic pathways.

Conclusion

Nucleic acids are versatile and attractive materials for constructing programmable and responsive elements in biomedicine, data storage, biocomputing, and nanotechnology. The ability to control nucleic acid structure and activity is essential in the design and implementation of such systems, and significant effort has been dedicated toward imparting stimuli-responsiveness in nucleic acid constructs. However, the majority of these efforts have focused on chemical or light-based reactivation of caged nucleic acids, and limitations remain in that these caging systems are not compatible with enzymatically-derived DNA substrates and have yet to be demonstrated with XNAs. As a third major stimuli source, heat remains surprisingly unexplored as a nucleic acid uncaging element, despite the high degree of control that is possible and its widespread use in laboratory settings.

In this work we show that glyoxal, a chemical denaturant used for decades in molecular biology assays, can impart thermoreversible inhibition of both the structure and activity of a variety of nucleic acid scaffolds. We first demonstrate facile glyoxal attachment on model DNA strands and show tunable addition of caging groups. We then extensively parameterize the removal of these cages through adjustable combinations of pH, temperature, and incubation times. Glyoxal cages are potent disruptors of nucleic acid secondary structure, and we show full inhibition of small molecule aptamer interactions as well as DNAzyme-based catalysis. In addition, because glyoxal reacts with nucleobase moieties rather than backbone functional groups, we show that thermoreversible caging can be easily applied toward natural DNA and RNA scaffolds as well as heavily modified backbones and non-canonical XNA polymers. We also explore glyoxal-based interference with enzyme activity, and identify several enzyme candidates that display reversible function

toward caged nucleic acid substrates, including several endonucleases as well as the CRISPR-Cas9 gene editing platform. Because glyoxalation is heat-reversible, we also demonstrate that caged primers provide significantly enhanced specificity in PCR amplification reactions. Lastly, we treat an antisense oligonucleotide with glyoxal and show that these constructs enable potent disruption of function as well as tunable activation and titration of gene expression levels in living mammalian cells. Together, we demonstrate that thermoreversible glyoxal caging can be easily applied for tunable inhibition and full reactivation of nucleic acid function in a suite of contexts, establishing a straightforward and effective framework for use in a variety of potential synthetic biology and biotechnology applications.

ASSOCIATED CONTENT

Supporting Information

General experimental protocols and additional data demonstrating caging and decaging kinetics and efficacy. The Supporting Information is available free of charge at pubs.acs.org.

AUTHOR INFORMATION

Corresponding Author

* jen.heemstra@emory.edu

Author Contributions

‡ S.D.K. and A.A.S. contributed equally.

Notes

The authors declare no competing financial interest.

ACKNOWLEDGMENT

This work was supported by the National Institutes of Health (R01GM116991 to J.M.H.), the Defense Threat Reduction Agency (HDTRA118-1-0029 to J.M.H.) and the National Science Foundation (DMR 1822262 and DMR 2003987 J.M.H.). We thank Mike Hanson and the oligonucleotide and peptide synthesis facility at the University of Utah for helpful advice and materials. This research project was also supported in part by the Emory University Integrated Cellular Imaging Microscopy Core, and we wish to thank Laura Fox-Goharioon for assistance in fluorescence imaging experiments.

REFERENCES

1. Seeman, N. C.; Sleiman, H. F., DNA nanotechnology. *Nature Reviews Materials* **2018,** *3* (1), 17068.
2. Guo, P., The emerging field of RNA nanotechnology. *Nature nanotechnology* **2010,** *5* (12), 833.
3. Wu, C.; Wan, S.; Hou, W.; Zhang, L.; Xu, J.; Cui, C.; Wang, Y.; Hu, J.; Tan, W., A survey of advancements in nucleic acid-based logic gates and computing for applications in biotechnology and biomedicine. *Chemical Communications* **2015,** *51* (18), 3723-3734.
4. Ganser, L. R.; Kelly, M. L.; Herschlag, D.; Al-Hashimi, H. M., The roles of structural dynamics in the cellular functions of RNAs. *Nature Reviews Molecular Cell Biology* **2019**, 1.
5. Höbartner, C.; Mittendorfer, H.; Breuker, K.; Micura, R., Triggering of RNA secondary structures by a functionalized nucleobase. *Angewandte Chemie International Edition* **2004,** *43* (30), 3922-3925.
6. Ikeda, M.; Kamimura, M.; Hayakawa, Y.; Shibata, A.; Kitade, Y., Reduction-Responsive Guanine Incorporated into G-Quadruplex-Forming DNA. *ChemBioChem* **2016,** *17* (14), 1304-1307.
7. Govan, J. M.; Young, D. D.; Lusic, H.; Liu, Q.; Lively, M. O.; Deiters, A., Optochemical control of RNA interference in mammalian cells. *Nucleic acids research* **2013,** *41* (22), 10518-10528.
8. Mikat, V.; Heckel, A., Light-dependent RNA interference with nucleobase-caged siRNAs. *Rna* **2007,** *13* (12), 2341-2347.
9. Lucas, T.; Schäfer, F.; Müller, P.; Eming, S. A.; Heckel, A.; Dimmeler, S., Light-inducible antimiR-92a as a therapeutic strategy to promote skin repair in healing-impaired diabetic mice. *Nature communications* **2017,** *8*, 15162.
10. Chaulk, S. G.; MacMillan, A. M., Synthesis of oligo-RNAs with photocaged adenosine 2′-hydroxyls. *Nature protocols* **2007,** *2* (5), 1052.
11. Matsushita-Ishiodori, Y.; Ohtsuki, T., Photoinduced RNA interference. *Accounts of chemical research* **2012,** *45* (7), 1039-1047.
12. Meyer, A.; Mokhir, A., RNA interference controlled by light of variable wavelength. *Angewandte Chemie* **2014,** *126* (47), 13054-13057.
13. Lu, J.; Koo, S. C.; Li, N.-S.; Piccirilli, J. A., Synthesis of 2′-O-Photocaged Ribonucleoside Phosphoramidites. *Nucleosides, Nucleotides and Nucleic Acids* **2015,** *34* (2), 114-129.
14. Tan, Z.; Feagin, T. A.; Heemstra, J. M., Temporal control of aptamer biosensors using covalent self-caging to shift equilibrium. *Journal of the American Chemical Society* **2016,** *138* (20), 6328-6331.
15. Kadina, A.; Kietrys, A. M.; Kool, E. T., RNA Cloaking by Reversible Acylation. *Angewandte Chemie International Edition* **2018,** *57* (12), 3059-3063.
16. Velema, W. A.; Kietrys, A. M.; Kool, E. T., RNA control by photoreversible acylation. *Journal of the American Chemical Society* **2018,** *140* (10), 3491-3495.
17. Durbeej, B.; Eriksson, L. A., Reaction mechanism of thymine dimer formation in DNA induced by UV light. *Journal of Photochemistry and Photobiology A: Chemistry* **2002,** *152* (1-3), 95-101.
18. Staehelin, M., Inactivation of virus nucleic acid with glyoxal derivatives. *Biochimica et biophysica acta* **1959,** *31* (2), 448-454.
19. Nakaya, K.; Takenaka, O.; Horinishi, H.; Shibata, K., Reactions of glyoxal with nucleic acids, nucleotides and their component bases. *Biochimica et Biophysica Acta (BBA)-Nucleic Acids and Protein Synthesis* **1968,** *161* (1), 23-31.
20. Shapiro, R.; Cohen, B. I.; Shiuey, S.-J.; Maurer, H., Reaction of guanine with glyoxal, pyruvaldehyde, and kethoxal, and the structure of the acylguanines. Synthesis of N2-alkylguanines. *Biochemistry* **1969,** *8* (1), 238-245.

21. Shapiro, R.; Cohen, B. I.; Clagett, D. C., Specific acylation of the guanine residues of ribonucleic acid. *Journal of Biological Chemistry* **1970,** *245* (10), 2633-2639.
22. Aubert, M.; Bellemare, G.; Monier, R., Selective reaction of glyoxal with guanine residues in native and denatured Escherichia coli 5S RNA. *Biochimie* **1973,** *55* (2), 135-142.
23. McMaster, G. K.; Carmichael, G. G., Analysis of single-and double-stranded nucleic acids on polyacrylamide and agarose gels by using glyoxal and acridine orange. *Proceedings of the National Academy of Sciences* **1977,** *74* (11), 4835-4838.
24. Murant, A.; Taylor, M.; Duncan, G.; Raschke, J., Improved estimates of molecular weight of plant virus RNA by agarose gel electrophoresis and electron microscopy after denaturation with glyoxal. *Journal of General Virology* **1981,** *53* (2), 321-332.
25. Bussolati, G.; Annaratone, L.; Berrino, E.; Miglio, U.; Panero, M.; Cupo, M.; Gugliotta, P.; Venesio, T.; Sapino, A.; Marchiò, C., Acid-free glyoxal as a substitute of formalin for structural and molecular preservation in tissue samples. *PloS one* **2017,** *12* (8), e0182965.
26. Weng, X.; Gong, J.; Chen, Y.; Wu, T.; Wang, F.; Yang, S.; Yuan, Y.; Luo, G.; Chen, K.; Hu, L., Keth-seq for transcriptome-wide RNA structure mapping. *Nature Chemical Biology* **2020,** *16* (5), 489-492.
27. Burnett, W. V., Northern blotting of RNA denatured in glyoxal without buffer recirculation. *BioTechniques* **1997,** *22* (4), 668-671.
28. Morse, D. P.; Bass, B. L., Detection of inosine in messenger RNA by inosine-specific cleavage. *Biochemistry* **1997,** *36* (28), 8429-8434.
29. Cattenoz, P. B.; Taft, R. J.; Westhof, E.; Mattick, J. S., Transcriptome-wide identification of A> I RNA editing sites by inosine specific cleavage. *Rna* **2013,** *19* (2), 257-270.
30. Gareau, D.; Desrosiers, A.; Vallée-Bélisle, A., Programmable quantitative DNA nanothermometers. *Nano letters* **2016,** *16* (7), 3976-3981.
31. Ke, G.; Wang, C.; Ge, Y.; Zheng, N.; Zhu, Z.; Yang, C. J., L-DNA molecular beacon: a safe, stable, and accurate intracellular nano-thermometer for temperature sensing in living cells. *Journal of the American Chemical Society* **2012,** *134* (46), 18908-18911.
32. Jonstrup, A. T.; Fredsøe, J.; Andersen, A. H., DNA hairpins as temperature switches, thermometers and ionic detectors. *Sensors* **2013,** *13* (5), 5937-5944.
33. Ebrahimi, S.; Akhlaghi, Y.; Kompany-Zareh, M.; Rinnan, Å., Nucleic acid based fluorescent nanothermometers. *ACS nano* **2014,** *8* (10), 10372-10382.
34. Modi, S.; Swetha, M.; Goswami, D.; Gupta, G. D.; Mayor, S.; Krishnan, Y., A DNA nanomachine that maps spatial and temporal pH changes inside living cells. *Nature nanotechnology* **2009,** *4* (5), 325-330.
35. Chen, X.; Chen, T.; Ren, L.; Chen, G.; Gao, X.; Li, G.; Zhu, X., Triplex DNA nanoswitch for pH-sensitive release of multiple cancer drugs. *ACS nano* **2019,** *13* (6), 7333-7344.
36. Deng, Y.; Ma, L.; Han, Q.; Yu, C.; Johnson-Buck, A.; Su, X., DNA-Templated Timer Probes for Multiplexed Sensing. *Nano Letters* **2020,** *20* (4), 2688-2694.
37. Schaffter, S. W.; Schulman, R., Building in vitro transcriptional regulatory networks by successively integrating multiple functional circuit modules. *Nature chemistry* **2019,** *11* (9), 829-838.
38. Filonov, G. S.; Moon, J. D.; Svensen, N.; Jaffrey, S. R., Broccoli: rapid selection of an RNA mimic of green fluorescent protein by fluorescence-based selection and directed evolution. *Journal of the American Chemical Society* **2014,** *136* (46), 16299-16308.
39. Wilson, S. C.; Cohen, D. T.; Wang, X. C.; Hammond, M. C., A neutral pH thermal hydrolysis method for quantification of structured RNAs. *Rna* **2014,** *20* (7), 1153-1160.
40. Santoro, S. W.; Joyce, G. F., A general purpose RNA-cleaving DNA enzyme. *Proceedings of the national academy of sciences* **1997,** *94* (9), 4262-4266.
41. Young, D. D.; Lively, M. O.; Deiters, A., Activation and deactivation of DNAzyme and antisense function with light for the photochemical regulation of gene expression in mammalian cells. *Journal of the American Chemical Society* **2010,** *132* (17), 6183-6193.
42. Hwang, K.; Wu, P.; Kim, T.; Lei, L.; Tian, S.; Wang, Y.; Lu, Y., Photocaged DNAzymes as a general method for sensing metal ions in living cells. *Angewandte Chemie International Edition* **2014,** *53* (50), 13798-13802.
43. Burmeister, P. E.; Lewis, S. D.; Silva, R. F.; Preiss, J. R.; Horwitz, L. R.; Pendergrast, P. S.; McCauley, T. G.; Kurz, J. C.; Epstein, D. M.; Wilson, C., Direct in vitro selection of a 2′-O-methyl aptamer to VEGF. *Chemistry & biology* **2005,** *12* (1), 25-33.
44. Zadeh, J. N.; Steenberg, C. D.; Bois, J. S.; Wolfe, B. R.; Pierce, M. B.; Khan, A. R.; Dirks, R. M.; Pierce, N. A., NUPACK: analysis and design of nucleic acid systems. *Journal of computational chemistry* **2011,** *32* (1), 170-173.
45. Schöning, K.-U.; Scholz, P.; Guntha, S.; Wu, X.; Krishnamurthy, R.; Eschenmoser, A., Chemical etiology of nucleic acid structure: the α-threofuranosyl-(3'→ 2') oligonucleotide system. *Science* **2000,** *290* (5495), 1347-1351.
46. Egholm, M.; Buchardt, O.; Nielsen, P. E.; Berg, R. H., Peptide nucleic acids (PNA). Oligonucleotide analogs with an achiral peptide backbone. *Journal of the American Chemical Society* **1992,** *114* (5), 1895-1897.
47. Jerabek-Willemsen, M.; André, T.; Wanner, R.; Roth, H. M.; Duhr, S.; Baaske, P.; Breitsprecher, D., MicroScale Thermophoresis: Interaction analysis and beyond. *Journal of Molecular Structure* **2014,** *1077*, 101-113.
48. Jacob, D.; Thüring, K.; Galliot, A.; Marchand, V.; Galvanin, A.; Ciftci, A.; Scharmann, K.; Stock, M.; Roignant, J. Y.; Leidel, S. A., Absolute quantification of noncoding RNA by microscale thermophoresis. *Angewandte Chemie International Edition* **2019**.

49. Wittung, P.; Nielsen, P. E.; Buchardt, O.; Egholm, M.; Norde, B., DNA-like double helix formed by peptide nucleic acid. *Nature* **1994,** *368* (6471), 561.
50. Miller, H. I.; Riggs, A. D.; Gill, G. N., Ribonuclease H (Hybrid) in Escherichia coli IDENTIFICATION AND CHARACTERIZATION. *Journal of Biological Chemistry* **1973,** *248* (7), 2621-2624.
51. Itaya, M.; Kondo, K., Molecular cloning of a ribonuclease H (RNase HI) gene from an extreme thermophile Thermus thermophilus HB8: a thermostable RNase H can functionally replace the Escherichia coli enzyme in vivo. *Nucleic acids research* **1991,** *19* (16), 4443-4449.
52. Findly, D.; Herries, D.; Mathias, A.; Rabin, B.; Ross, C., The active site and mechanism of action of bovine pancreatic ribonuclease. *Nature* **1961,** *190* (4778), 781-784.
53. Fujimoto, M.; Kuninaka, A.; Yoshino, H., Substrate specificity of nuclease P1. *Agricultural and Biological Chemistry* **1974,** *38* (9), 1555-1561.
54. Vanecko, S.; Laskowski Sr, M., Studies of the specificity of deoxyribonuclease I. II. Hydrolysis of oligonucleotides carrying a monoesterified phosphate on carbon 3'. *Journal of Biological Chemistry (US)* **1961,** *236*.
55. Deutscher, M. P.; Marlor, C. W.; Zaniewski, R., Ribonuclease T: new exoribonuclease possibly involved in end-turnover of tRNA. *Proceedings of the National Academy of Sciences* **1984,** *81* (14), 4290-4293.
56. Viswanathan, M.; Lanjuin, A.; Lovett, S. T., Identification of RNase T as a high-copy suppressor of the UV sensitivity associated with single-strand DNA exonuclease deficiency in Escherichia coli. *Genetics* **1999,** *151* (3), 929-934.
57. Williams, E. J.; Sung, S.-C.; Laskowski, M., Action of venom phosphodiesterase on deoxyribonucleic acid. *Journal of Biological Chemistry* **1961,** *236* (4), 1130-1134.
58. Jinek, M.; Chylinski, K.; Fonfara, I.; Hauer, M.; Doudna, J. A.; Charpentier, E., A programmable dual-RNA–guided DNA endonuclease in adaptive bacterial immunity. *science* **2012,** *337* (6096), 816-821.
59. Cong, L.; Ran, F. A.; Cox, D.; Lin, S.; Barretto, R.; Habib, N.; Hsu, P. D.; Wu, X.; Jiang, W.; Marraffini, L. A., Multiplex genome engineering using CRISPR/Cas systems. *Science* **2013,** *339* (6121), 819-823.
60. Zhou, W.; Brown, W.; Bardhan, A.; Delaney, M.; Ilk, A. S.; Rauen, R. R.; Kahn, S. I.; Tsang, M.; Deiters, A., Spatiotemporal Control of CRISPR/Cas9 Function in Cells and Zebrafish using Light-Activated Guide RNA. *bioRxiv* **2019**, 831974.
61. Wang, S.-R.; Wu, L.-Y.; Huang, H.-Y.; Xiong, W.; Liu, J.; Wei, L.; Yin, P.; Tian, T.; Zhou, X., Conditional control of RNA-guided nucleic acid cleavage and gene editing. *Nature Communications* **2020,** *11* (1), 1-10.
62. Habibian, M.; McKinlay, C.; Blake, T. R.; Kietrys, A. M.; Waymouth, R. M.; Wender, P. A.; Kool, E. T., Reversible RNA acylation for control of CRISPR–Cas9 gene editing. *Chemical Science* **2020**.
63. Lin, B.; An, Y.; Meng, L.; Zhang, H.; Song, J.; Zhu, Z.; Liu, W.; Song, Y.; Yang, C., Control of CRISPR-Cas9 with small molecule-activated allosteric aptamer regulating sgRNAs. *Chemical Communications* **2019,** *55* (81), 12223-12226.
64. Raper, A. T.; Stephenson, A. A.; Suo, Z., Functional insights revealed by the kinetic mechanism of CRISPR/Cas9. *Journal of the American Chemical Society* **2018,** *140* (8), 2971-2984.
65. Konermann, S.; Brigham, M. D.; Trevino, A. E.; Joung, J.; Abudayyeh, O. O.; Barcena, C.; Hsu, P. D.; Habib, N.; Gootenberg, J. S.; Nishimasu, H., Genome-scale transcriptional activation by an engineered CRISPR-Cas9 complex. *Nature* **2015,** *517* (7536), 583.
66. Qi, L. S.; Larson, M. H.; Gilbert, L. A.; Doudna, J. A.; Weissman, J. S.; Arkin, A. P.; Lim, W. A., Repurposing CRISPR as an RNA-guided platform for sequence-specific control of gene expression. *Cell* **2013,** *152* (5), 1173-1183.
67. Komor, A. C.; Kim, Y. B.; Packer, M. S.; Zuris, J. A.; Liu, D. R., Programmable editing of a target base in genomic DNA without double-stranded DNA cleavage. *Nature* **2016,** *533* (7603), 420-424.
68. Anzalone, A. V.; Randolph, P. B.; Davis, J. R.; Sousa, A. A.; Koblan, L. W.; Levy, J. M.; Chen, P. J.; Wilson, C.; Newby, G. A.; Raguram, A., Search-and-replace genome editing without double-strand breaks or donor DNA. *Nature* **2019,** *576* (7785), 149-157.
69. Rauch, S.; He, E.; Srienc, M.; Zhou, H.; Zhang, Z.; Dickinson, B. C., Programmable RNA-guided RNA effector proteins built from human parts. *Cell* **2019,** *178* (1), 122-134. e12.
70. Wang, A. M.; Doyle, M. V.; Mark, D. F., Quantitation of mRNA by the polymerase chain reaction. *Proceedings of the National Academy of Sciences* **1989,** *86* (24), 9717-9721.
71. Chan, J. F.-W.; Yip, C. C.-Y.; To, K. K.-W.; Tang, T. H.-C.; Wong, S. C.-Y.; Leung, K.-H.; Fung, A. Y.-F.; Ng, A. C.-K.; Zou, Z.; Tsoi, H.-W., Improved molecular diagnosis of COVID-19 by the novel, highly sensitive and specific COVID-19-RdRp/Hel real-time reverse transcription-PCR assay validated in vitro and with clinical specimens. *Journal of Clinical Microbiology* **2020,** *58* (5).
72. Rychlik, W., Selection of primers for polymerase chain reaction. *Molecular biotechnology* **1995,** *3* (2), 129-134.
73. Kellogg, D.; Rybalkin, I.; Chen, S.; Mukhamedova, N.; Vlasik, T.; Siebert, P.; Chenchik, A., TaqStart Antibody:" hot start" PCR facilitated by a neutralizing monoclonal antibody directed against Taq DNA polymerase. *Biotechniques* **1994,** *16* (6), 1134-1137.
74. Lin, Y.; Jayasena, S. D., Inhibition of multiple thermostable DNA polymerases by a heterodimeric aptamer. *Journal of molecular biology* **1997,** *271* (1), 100-111.

75. Young, D. D.; Edwards, W. F.; Lusic, H.; Lively, M. O.; Deiters, A., Light-triggered polymerase chain reaction. *Chemical communications* **2008,** (4), 462-464.
76. Lebedev, A. V.; Paul, N.; Yee, J.; Timoshchuk, V. A.; Shum, J.; Miyagi, K.; Kellum, J.; Hogrefe, R. I.; Zon, G., Hot start PCR with heat-activatable primers: a novel approach for improved PCR performance. *Nucleic acids research* **2008,** *36* (20), e131-e131.
77. Jost, M.; Santos, D. A.; Saunders, R. A.; Horlbeck, M. A.; Hawkins, J. S.; Scaria, S. M.; Norman, T. M.; Hussmann, J. A.; Liem, C. R.; Gross, C. A., Titrating gene expression using libraries of systematically attenuated CRISPR guide RNAs. *Nature Biotechnology* **2020,** *38* (3), 355-364.
78. Michaels, Y. S.; Barnkob, M. B.; Barbosa, H.; Baeumler, T. A.; Thompson, M. K.; Andre, V.; Colin-York, H.; Fritzsche, M.; Gileadi, U.; Sheppard, H. M., Precise tuning of gene expression levels in mammalian cells. *Nature communications* **2019,** *10* (1), 1-12.
79. Castanotto, D.; Lin, M.; Kowolik, C.; Wang, L.; Ren, X.-Q.; Soifer, H. S.; Koch, T.; Hansen, B. R.; Oerum, H.; Armstrong, B., A cytoplasmic pathway for gapmer antisense oligonucleotide-mediated gene silencing in mammalian cells. *Nucleic acids research* **2015,** *43* (19), 9350-9361.
80. Liang, X.-H.; Sun, H.; Nichols, J. G.; Crooke, S. T., RNase H1-dependent antisense oligonucleotides are robustly active in directing RNA cleavage in both the cytoplasm and the nucleus. *Molecular Therapy* **2017,** *25* (9), 2075-2092.
81. Stein, C.; Hansen, J. B.; Lai, J.; Wu, S.; Voskresenskiy, A.; H∅ g, A.; Worm, J.; Hedtjärn, M.; Souleimanian, N.; Miller, P., Efficient gene silencing by delivery of locked nucleic acid antisense oligonucleotides, unassisted by transfection reagents. *Nucleic acids research* **2010,** *38* (1), e3-e3.
82. Petersen, M.; Wengel, J., LNA: a versatile tool for therapeutics and genomics. *Trends in biotechnology* **2003,** *21* (2), 74-81.
83. Lim, K. R. Q.; Maruyama, R.; Echigoya, Y.; Nguyen, Q.; Zhang, A.; Khawaja, H.; Chandra, S. S.; Jones, T.; Jones, P.; Chen, Y.-W., Inhibition of DUX4 expression with antisense LNA gapmers as a therapy for facioscapulohumeral muscular dystrophy. *Proceedings of the National Academy of Sciences* **2020,** *117* (28), 16509-16515.
84. Zimmer, M., Green fluorescent protein (GFP): applications, structure, and related photophysical behavior. *Chemical reviews* **2002,** *102* (3), 759-782.
85. He, L.; Binari, R.; Huang, J.; Falo-Sanjuan, J.; Perrimon, N., In vivo study of gene expression with an enhanced dual-color fluorescent transcriptional timer. *Elife* **2019,** *8*, e46181.
86. Corish, P.; Tyler-Smith, C., Attenuation of green fluorescent protein half-life in mammalian cells. *Protein engineering* **1999,** *12* (12), 1035-1040.
87. Kiełpiński, Ł. J.; Hagedorn, P. H.; Lindow, M.; Vinther, J., RNase H sequence preferences influence antisense oligonucleotide efficiency. *Nucleic acids research* **2017,** *45* (22), 12932-12944.
88. Magner, D.; Biala, E.; Lisowiec-Wachnicka, J.; Kierzek, R., Influence of mismatched and bulged nucleotides on SNP-preferential RNase H cleavage of RNA-antisense gapmer heteroduplexes. *Scientific reports* **2017,** *7* (1), 1-16.
89. Nowotny, M.; Gaidamakov, S. A.; Crouch, R. J.; Yang, W., Crystal structures of RNase H bound to an RNA/DNA hybrid: substrate specificity and metal-dependent catalysis. *Cell* **2005,** *121* (7), 1005-1016.
90. Grishagin, I. V., Automatic cell counting with ImageJ. *Analytical biochemistry* **2015,** *473*, 63-65.
91. Asokan, A.; Cho, M. J., Exploitation of intracellular pH gradients in the cellular delivery of macromolecules. *Journal of pharmaceutical sciences* **2002,** *91* (4), 903-913.
92. Näreoja, T.; Deguchi, T.; Christ, S.; Peltomaa, R.; Prabhakar, N.; Fazeli, E.; Perälä, N.; Rosenholm, J. M.; Arppe, R.; Soukka, T., Ratiometric sensing and imaging of intracellular pH using polyethylenimine-coated photon upconversion nanoprobes. *Analytical chemistry* **2017,** *89* (3), 1501-1508.
93. Kulkarni, C.; Nadtochiy, S. M.; Kennedy, L.; Zhang, J.; Chhim, S.; Alwaseem, H.; Murphy, E.; Fu, D.; Brookes, P. S., ALKBH7 mediates necrosis via rewiring of glyoxal metabolism. *bioRxiv* **2020**.
94. Lee, C.; Kim, I.; Lee, J.; Lee, K.-L.; Min, B.; Park, C., Transcriptional activation of the aldehyde reductase YqhD by YqhC and its implication in glyoxal metabolism of Escherichia coli K-12. *Journal of bacteriology* **2010,** *192* (16), 4205-4214.
95. Mlakar, A.; Batna, A.; Dudda, A.; Spiteller, G., Iron (II) ions induced oxidation of ascorbic acid and glucose. *Free radical research* **1996,** *25* (6), 525-539.
96. Sliman, S. M.; Eubank, T. D.; Kotha, S. R.; Kuppusamy, M. L.; Sherwani, S. I.; Butler, E. S. O. C.; Kuppusamy, P.; Roy, S.; Marsh, C. B.; Stern, D. M., Hyperglycemic oxoaldehyde, glyoxal, causes barrier dysfunction, cytoskeletal alterations, and inhibition of angiogenesis in vascular endothelial cells: aminoguanidine protection. *Molecular and cellular biochemistry* **2010,** *333* (1-2), 9-26.
97. Shangari, N.; O'Brien, P. J., The cytotoxic mechanism of glyoxal involves oxidative stress. *Biochemical pharmacology* **2004,** *68* (7), 1433-1442.
98. Tominaga, H.; Ishiyama, M.; Ohseto, F.; Sasamoto, K.; Hamamoto, T.; Suzuki, K.; Watanabe, M., A water-soluble tetrazolium salt useful for colorimetric cell viability assay. *Analytical Communications* **1999,** *36* (2), 47-50.

Insert Table of Contents artwork here